PERFORMANCE ANALYSIS OF A MACH–ZEHNDER INTERFEROMETER USING SYNTHETIC INTERFEROGRAMS

F. Alharthi *[1,2,3], D. Graham[1,3], M. Hibberd[1,3], and Ö. Apsimon[1,3]
[1]The University of Manchester, Manchester, United Kingdom
[2]University of Bisha, Bisha, Saudi Arabia
[3]Cockcroft Institute of Accelerator Science and Technology, Daresbury, United Kingdom

Abstract

In this work, we assess the performance and limitations of Mach–Zehnder interferometry for plasma diagnostics using a fully synthetic, numerically generated dataset. We explore regions of parameter space that are difficult to access experimentally, including fringe behaviour, the dynamic range of measurable phase shifts, and the resolution limits for low-density plasmas. By introducing controlled phase errors, we quantify the robustness of common phase retrieval and phase unwrapping algorithms and identify the conditions under which these methods succeed or fail. Our results provide practical design guidelines for optimising interferometric measurements across a wide range of plasma conditions.

INTRODUCTION

In 1979, Tajima and Dawson proposed using plasma waves to accelerate charged particles [1], demonstrating that plasma could generate electric fields thousands of times stronger than those used in conventional accelerators. This remained theoretical until 1988, when Rosenzweig and his team experimentally proved it for the first time [2], paving the way for a new generation of accelerators.

The field then advanced significantly through pioneering experiments at the Berkeley Lab Laser Accelerator (BELLA) facility, which demonstrated the use of plasma channels for laser-driven wakefield acceleration. The first GeV-class electron beam was achieved in 2006 using a capillary discharge plasma channel [3], and subsequent improvements led to the acceleration of electrons up to 7.8 GeV in a 20-cm-long channel [4]. A key advancement was the development of laser-heated capillary channels, in which an auxiliary laser is used to shape the radial plasma density profile, enabling efficient guiding of the drive laser over long distances distances [4]. In all these experiments, precise measurement of plasma density plays a crucial role, and the Mach–Zehnder interferometer (MZI) is one of the most common instruments used for this purpose. However, its accuracy depends on phase-recovery algorithms and is affected by physical limitations such as phase wrapping at high densities. In this work, we evaluate the performance and limitations of the MZI using a fully synthetic dataset, and we investigate the effect of plasma density, spectral window selection and width, and probe beam wavelength on retrieval accuracy.

* fatimah.alharthi@postgrad.manchester.ac.uk

METHODOLOGY

Synthetic Interferograms

A fully synthetic dataset of Mach–Zehnder interferograms was generated so that the plasma phase is known exactly (see Fig. 1), allowing the retrieval algorithm to be tested independently of experimental noise. Each interferogram was simulated on a 1024×1024 grid with pixel size $\Delta x = 1.75\,\mu\text{m}$ (field of view $L \approx 1.79$ mm). The plasma was modelled as a cylinder of radius $R = 400\,\mu\text{m}$ with axis along y (parallel to the carrier fringes) and perpendicular to the probe direction z, with a parabolic radial profile $n_e(r) = n_{e0}(1-r^2/R^2)$, where $r = \sqrt{x^2 + z^2}$. Translational invariance along y implies that the line-integrated density $N_e(x) = \int n_e\, dz$ depends only on x.

In the regime $n_e \ll n_c$, where $n_c = \varepsilon_0 m_e \omega^2/e^2$ is the critical density at which the plasma frequency ω_{pe} equals the probe angular frequency ω, the phase shift reduces to

$$\Delta\varphi(x) = -r_e \lambda\, N_e(x), \tag{1}$$

with $r_e = 2.818 \times 10^{-15}$ m the classical electron radius and $\lambda = 532$ nm the probe wavelength (frequency-doubled Nd:YAG). Interferograms were constructed as $I = \frac{1}{2}[1 + \cos(2\pi f_0 x + \Delta\varphi)]$, with $\Delta\varphi = 0$ for the reference, and n_{e0} was scanned over 10^{15}–10^{20} cm^{-3}.

Phase Retrieval and Density Extraction

The plasma-induced phase was recovered using the Fourier-Transform Method (FTM) [5]. Since $\Delta\varphi$ is invariant along y, the 2D interferograms were averaged column-wise into 1D traces $g_{\text{pl}}(x)$ and $g_{\text{ref}}(x)$. An FFT of each trace yields a DC peak and two sidebands at $\pm f_0$ (Fig. 2); the positive sideband is isolated with a spectral window centred on $+f_0$. Four window types (Hann, Gaussian, Tukey, super-Gaussian) and a range of widths were tested. After shifting the filtered sideband to the origin and applying an inverse FFT, the wrapped phase is obtained from the argument of the complex ratio, which cancels the carrier and any residual phase. The unwrapped phase (Fig. 3) is inverted using Eq. (1) to obtain $N_e(x)$, and a three-point Abel transform [6] recovers $n_e(r)$. The relative error between retrieved and input peak densities is used as the performance metric, with a 5% threshold defining the failure point.

RESULTS AND DISCUSSION

Interferograms were generated across an electron density range from 10^{15} to 10^{20} cm^{-3} using an 800 nm probe. The

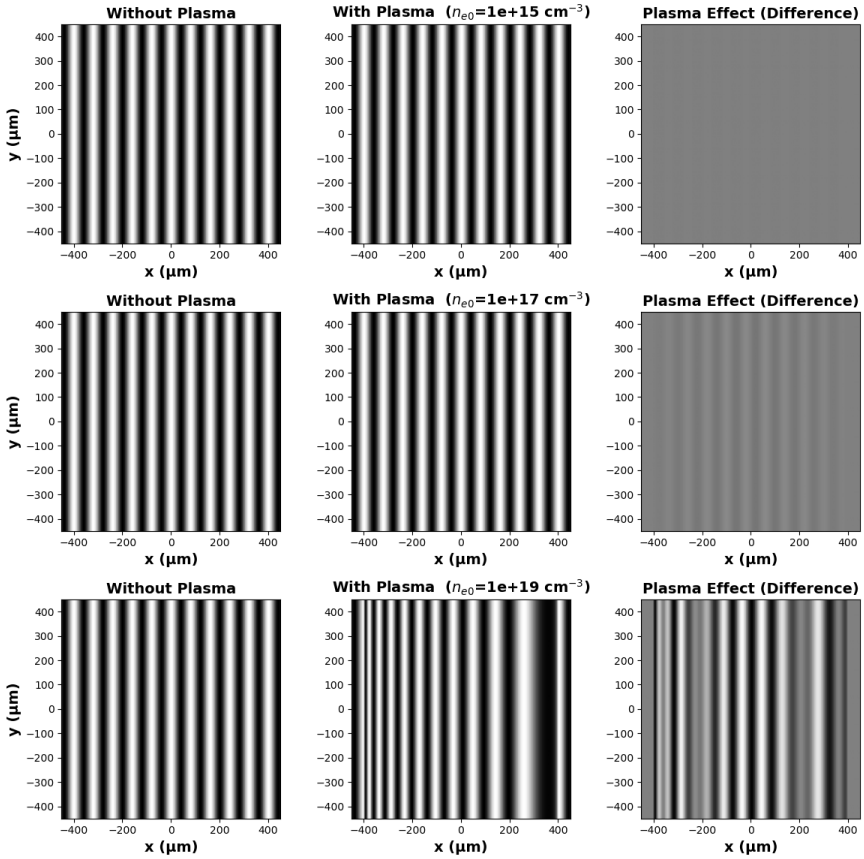

Figure 1: Synthetic interferograms generated for three representative plasma densities: a low value $n_{e0} = 10^{15}$ cm^{-3}, an intermediate value $n_{e0} = 10^{17}$ cm^{-3}, and a high value $n_{e0} = 10^{19}$ cm^{-3}.

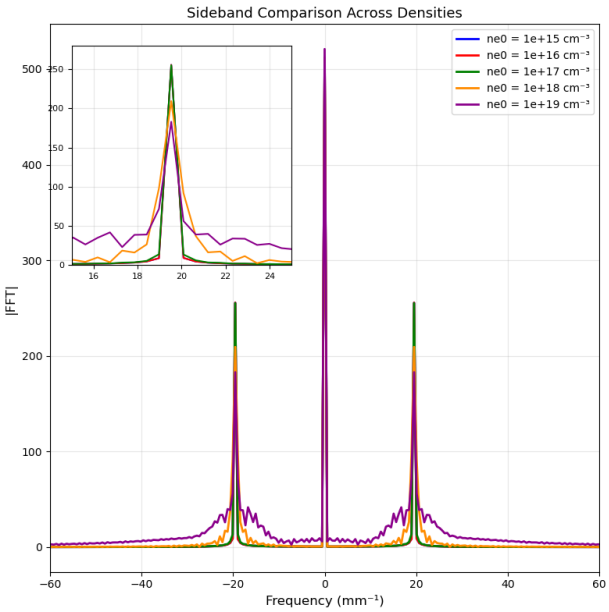

Figure 2: Fourier spectrum of the plasma interferogram for different peak densities. The two side bands at $\pm f_0 \approx 20$ mm^{-1} carry the phase information.

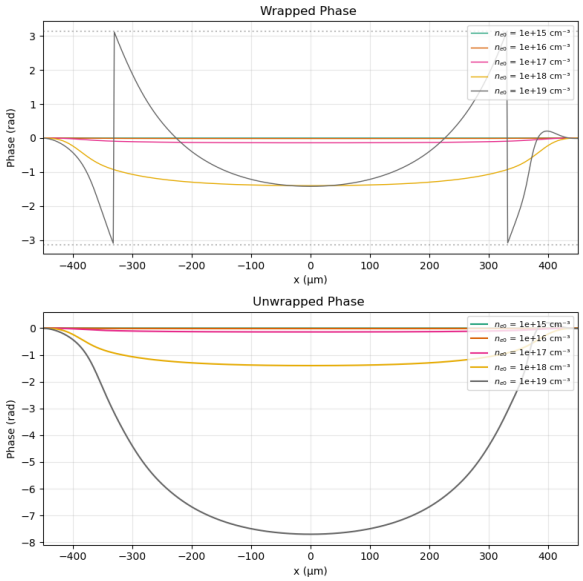

Figure 3: Wrapped (top) and unwrapped (bottom). At $n_{e0} = 10^{19}$ cm^{-3} the cumulative phase exceeds 2π, so unwrapping is required to recover the true monotonic profile.

phase is recovered with high accuracy below $\sim 10^{19}$ cm^{-3} (error less than 5%), after which a sharp transition occurs, causing the error to rise above 10% and rendering the recovery unreliable. This breakdown is explained by the linear relationship between phase shift and density ($\Delta\varphi \propto$

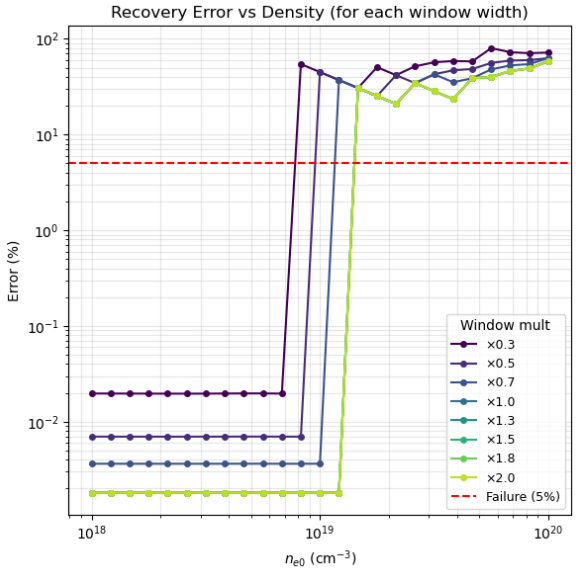

Figure 4: Recovery error versus plasma density for different spectral window widths; wider windows improve precision but do not shift the breakdown point.

$\int n_e\, dl/\lambda$): the wrapping limit $\Delta\varphi = \pi$ is reached near 2×10^{18} cm^{-3}, and beyond $\Delta\varphi = 2\pi$ the fringes fold into the interval $[-\pi, \pi]$ and the unwrapping algorithm fails to recover the original profile.

The window width was varied from 0.3× to 2.0× the nominal value (Fig. 4). Wider windows improve accuracy in the lower range (from ~ 0.02% at 0.3× to ~ 0.002% at 2.0×), but all fail within a narrow range between 7×10^{18} and 1.5×10^{19} cm^{-3}. Widening the window therefore only improves accuracy and does not raise the upper limit of measurement.

Seven wavelengths from 266 nm (4ω Nd:YAG) to 10.6 µm (CO_2 laser) were investigated (Fig. 5). Shorter wavelengths extend the retrieval range to higher densities: a 266 nm probe reaches ~ 3×10^{19} cm^{-3}, while the 10.6 µm probe fails across the entire range. The breakdown location follows the critical-density relation $n_c \propto 1/\lambda^2$, confirming that wavelength imposes the true measurement ceiling.

CONCLUSIONS

A fully synthetic Mach–Zehnder framework was used to map the operational envelope of Fourier-based phase retrieval across plasma density, window function, window width, and probe wavelength. The recovery remains accurate (error < 0.01%) until a sharp breakdown occurs at a wavelength-dependent threshold following the critical-density scaling $n_c \propto 1/\lambda^2$, indicating that the upper limit might be set by the underlying physics rather than by algorithmic choices. Window shape and width affect precision but not the breakdown point, while the probe wavelength imposes the true measurement ceiling.

Future work will extend this study by introducing realistic noise sources and investigating additional effects such as plasma profile shape, recovery limit, and probe beam imperfections, in order to assess the robustness of the retrieval under experimentally relevant conditions.

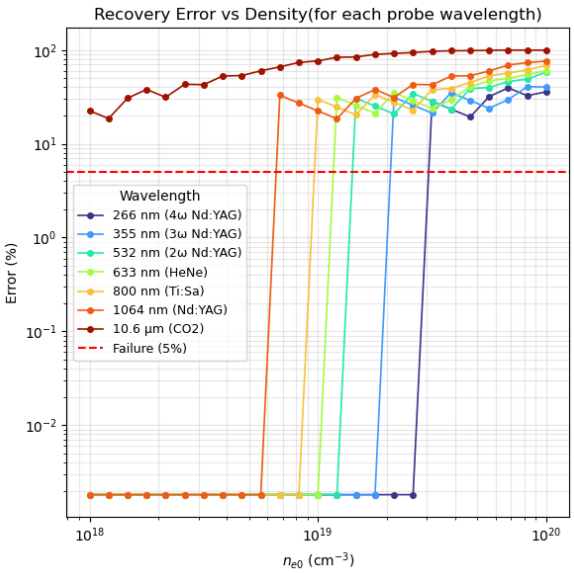

Figure 5: Recovery error versus plasma density for seven probe wavelengths; the breakdown follows the scaling $n_c \propto 1/\lambda^2$.

REFERENCES

[1] T. Tajima and J. M. Dawson, "Laser Electron Accelerator", *Phys. Rev. Lett.*, vol. 43, no. 4, pp. 267–270, 1979. doi:10.1103/PhysRevLett.43.267

[2] J. B. Rosenzweig *et al.*, "Experimental observation of plasma wake-field acceleration", *Phys. Rev. Lett.*, vol. 61, no. 1, pp. 98–101, 1988. doi:10.1103/PhysRevLett.61.98

[3] W. P. Leemans *et al.*, "Gev electron beams from a centimetre-scale accelerator", *Nat. Phys.*, vol. 2, pp. 696–699, 2006. doi:10.1038/nphys418

[4] A. J. Gonsalves *et al.*, "Petawatt Laser Guiding and Electron Beam Acceleration to 8 GeV in a Laser-Heated Capillary Discharge Waveguide", *Phys. Rev. Lett.*, vol. 122, p. 084801, 2019. doi:10.1103/PhysRevLett.122.084801

[5] M. Takeda, H. Ina, and S. Kobayashi, "Fourier-Transform Method of Fringe-Pattern Analysis for Computer-Based Topography and Interferometry", *J. Opt. Soc. Amer.*, vol. 72, no. 1, pp. 156–160, 1982. doi:10.1364/JOSA.72.000156

[6] S. Lee *et al.*, "Interferometry analysis with fringe normalization and matrix Abel inversion for plasma diagnostics", *J. Instrum.*, vol. 18, p. C12016, 2023. doi:10.1088/1748-0221/18/12/C12016